

2016

# Resolving the HONO formation mechanism in the ionosphere via ab initio molecular dynamic simulations

Rongxing He  
*Southwest University*

Lei Li  
*University of Nebraska-Lincoln*


Jie Zhong  
*University of Nebraska-Lincoln, jzhong4@unl.edu*

Chongqin Zhu  
*University of Nebraska-Lincoln*

Joseph S. Francisco  
*University of Nebraska-Lincoln, frjoseph@sas.upenn.edu*

*See next page for additional authors*

Follow this and additional works at: <https://digitalcommons.unl.edu/chemzeng>

 Part of the [Analytical Chemistry Commons](#), [Materials Chemistry Commons](#), and the [Physical Chemistry Commons](#)

---

He, Rongxing; Li, Lei; Zhong, Jie; Zhu, Chongqin; Francisco, Joseph S.; and Zeng, Xiao Cheng, "Resolving the HONO formation mechanism in the ionosphere via ab initio molecular dynamic simulations" (2016). *Xiao Cheng Zeng Publications*. 153.  
<https://digitalcommons.unl.edu/chemzeng/153>

This Article is brought to you for free and open access by the Published Research - Department of Chemistry at DigitalCommons@University of Nebraska - Lincoln. It has been accepted for inclusion in Xiao Cheng Zeng Publications by an authorized administrator of DigitalCommons@University of Nebraska - Lincoln.

---

**Authors**

Rongxing He, Lei Li, Jie Zhong, Chongqin Zhu, Joseph S. Francisco, and Xiao Cheng Zeng

# Resolving the HONO formation mechanism in the ionosphere via ab initio molecular dynamic simulations

Rongxing He<sup>a,b,1</sup>, Lei Li<sup>b,1</sup>, Jie Zhong<sup>b</sup>, Chongqin Zhu<sup>b</sup>, Joseph S. Francisco<sup>b,2</sup>, and Xiao Cheng Zeng<sup>b,2</sup>

<sup>a</sup>Key Laboratory of Luminescence and Real-Time Analytical Chemistry, Ministry of Education, College of Chemistry and Chemical Engineering, Southwest University, Chongqing 400715, China; and <sup>b</sup>Department of Chemistry, University of Nebraska–Lincoln, Lincoln, NE 68588

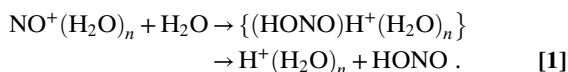
Contributed by Joseph S. Francisco, February 2, 2016 (sent for review November 3, 2015; reviewed by Hua Guo and Ryan P. Steele)

**Solar emission produces copious nitrosonium ions (NO<sup>+</sup>) in the D layer of the ionosphere, 60 to 90 km above the Earth's surface. NO<sup>+</sup> is believed to transfer its charge to water clusters in that region, leading to the formation of gaseous nitrous acid (HONO) and protonated water cluster. The dynamics of this reaction at the ionospheric temperature (200–220 K) and the associated mechanistic details are largely unknown. Using ab initio molecular dynamics (AIMD) simulations and transition-state search, key structures of the water hydrates—tetrahydrate NO<sup>+</sup>(H<sub>2</sub>O)<sub>4</sub> and pentahydrate NO<sup>+</sup>(H<sub>2</sub>O)<sub>5</sub>—are identified and shown to be responsible for HONO formation in the ionosphere. The critical tetrahydrate NO<sup>+</sup>(H<sub>2</sub>O)<sub>4</sub> exhibits a chain-like structure through which all of the lowest-energy isomers must go. However, most lowest-energy isomers of pentahydrate NO<sup>+</sup>(H<sub>2</sub>O)<sub>5</sub> can be converted to the HONO-containing product, encountering very low barriers, via a chain-like or a three-armed, star-like structure. Although these structures are not the global minima, at 220 K, most lowest-energy NO<sup>+</sup>(H<sub>2</sub>O)<sub>4</sub> and NO<sup>+</sup>(H<sub>2</sub>O)<sub>5</sub> isomers tend to channel through these highly populated isomers toward HONO formation.**

ionosphere | HONO | mechanism | water | clusters

The ionosphere is the largest layer in the Earth's atmosphere, ranging in altitude from ~60 to 1,000 km and includes the thermosphere and parts of the mesosphere and exosphere. The ionosphere contains a high concentration of electrons and ions because of the ionization of gases in that region by short wavelength radiation from the Sun. Therefore, these species play an important role in atmospheric electricity, influencing radio propagation to different regions on the Earth's surface and space-based navigational systems (1). The D layer is the innermost layer of the ionosphere, ranging from 60 to 90 km in altitude, where Lyman series- $\alpha$  hydrogen radiation from the Sun gives rise to abundant nitrosonium ions (NO<sup>+</sup>). In addition to the ionospheric reaction between NO<sup>+</sup> and water, explorations of the chemical reactivity of NO<sup>+</sup> and water clusters (2–4) have implications for understanding the mechanisms of atmospherically relevant reactions in water clusters (5–9).

Over the past two decades, several experimental and theoretical studies (10–13) have focused on understanding the chemical and physical properties of the small-sized hydrated nitrosonium ion NO<sup>+</sup>(H<sub>2</sub>O)<sub>*n*</sub>, where *n* = 1–5. Two key processes have been proposed for HONO formation:



Lee and coworkers (14) used vibrational spectroscopy to obtain clear evidence of the rearrangement of the NO<sup>+</sup>(H<sub>2</sub>O)<sub>*n*</sub> cluster by observing the appearance of new hydrogen (H)-bonded OH stretching lines. Using quantum molecular dynamics, Ye and Cheng (15) suggested possible structures and corresponding IR spectra for NO<sup>+</sup>(H<sub>2</sub>O)<sub>*n*</sub> (*n* = 1–3) clusters. In a major experimental breakthrough, Relph et al. (16) showed that the extent to which reaction 1 produces HONO and H<sup>+</sup>(H<sub>2</sub>O)<sub>*n*</sub> depends on the size and shape of the water clusters. Another key finding was that the reactions for HONO production start with the *n* = 4 water cluster.

Later, the importance of the tetrahydrate isomer NO<sup>+</sup>(H<sub>2</sub>O)<sub>4</sub> to its conversion to proton hydrate and HONO at temperature beyond 150 K was further demonstrated experimentally by Eyet et al. (11). Indeed, before Eyet's study, Siefermann and Abel (17) had already noted that the configurations of the trihydrate and tetrahydrate isomers examined in Relph et al.'s experiment were frozen because of the very low temperature used (5 K). At this low temperature, the most abundant water cluster structures are those found at the global minima of the potential energy surface. At temperatures that are relevant to the ionosphere (200–220 K), these lowest-lying isomers may not directly contribute to the interconversion processes involving the hydrated NO<sup>+</sup>(H<sub>2</sub>O)<sub>*n*</sub> ion.

An early study suggested that the low rate of reaction 1 can be attributed to the fact that the reactive species responsible for HONO formation include a higher-energy isomer of NO<sup>+</sup>(H<sub>2</sub>O)<sub>*n*</sub> that is responsible to the release of a proton (12). Asada et al. (18) reported high-level ab initio molecular-orbital calculations and identified tens of low-energy isomers of NO<sup>+</sup>(H<sub>2</sub>O)<sub>4</sub> and NO<sup>+</sup>(H<sub>2</sub>O)<sub>5</sub>. They also pointed out that relatively higher-energy reactant, transition-state, and product isomers are involved in the formation of HONO from NO<sup>+</sup>(H<sub>2</sub>O)<sub>*n*</sub> (*n* = 4 and 5) clusters. But, the nature of the mechanism by which these relatively higher-energy isomers (in the frozen state at 0 K) can directly contribute to the interconversion processes at temperatures relevant to the ionosphere is little studied.

In light of the lack of experimental studies of the dynamics of isomer transformation, we performed Born–Oppenheimer ab initio molecular dynamics (AIMD) simulations to explore the dynamic behaviors of trihydrate NO<sup>+</sup>(H<sub>2</sub>O)<sub>3</sub>, tetrahydrate NO<sup>+</sup>(H<sub>2</sub>O)<sub>4</sub>, and pentahydrate NO<sup>+</sup>(H<sub>2</sub>O)<sub>5</sub> clusters at 220 K. Our results suggest that 220 K is adequate to drive the isomer interconversion from the

## Significance

This contribution resolves a long-standing puzzle of the nitrous acid (HONO) formation mechanism from NO<sup>+</sup> motif and water clusters in the ionosphere (key layer for radio signal transmission). From previous studies, massive different isomer structures have been identified. However, an explanation of how the low-lying isomers channel through the high-lying ones to form HONO species has been elusive. A clear understanding of the mechanism was only possible through molecular dynamics simulation. This work identifies the critical isomer that is key to linking the network of all the low-lying isomers together. This finding provides, to our knowledge, the first solid theoretical evidence for the formation of HONO in the ionosphere.

Author contributions: R.H., L.L., J.S.F., and X.C.Z. designed research; R.H., L.L., J.Z., C.Z., and X.C.Z. performed research; R.H., L.L., J.Z., C.Z., J.S.F., and X.C.Z. analyzed data; and R.H., L.L., J.S.F., and X.C.Z. wrote the paper.

Reviewers: H.G., University of New Mexico; and R.P.S., University of Utah.

The authors declare no conflict of interest.

<sup>1</sup>R.H. and L.L. contributed equally to this work.

<sup>2</sup>To whom correspondence may be addressed. Email: jfrancisco3@unl.edu or xzeng1@unl.edu.

This article contains supporting information online at [www.pnas.org/lookup/suppl/doi:10.1073/pnas.1601651113/-DCSupplemental](http://www.pnas.org/lookup/suppl/doi:10.1073/pnas.1601651113/-DCSupplemental).

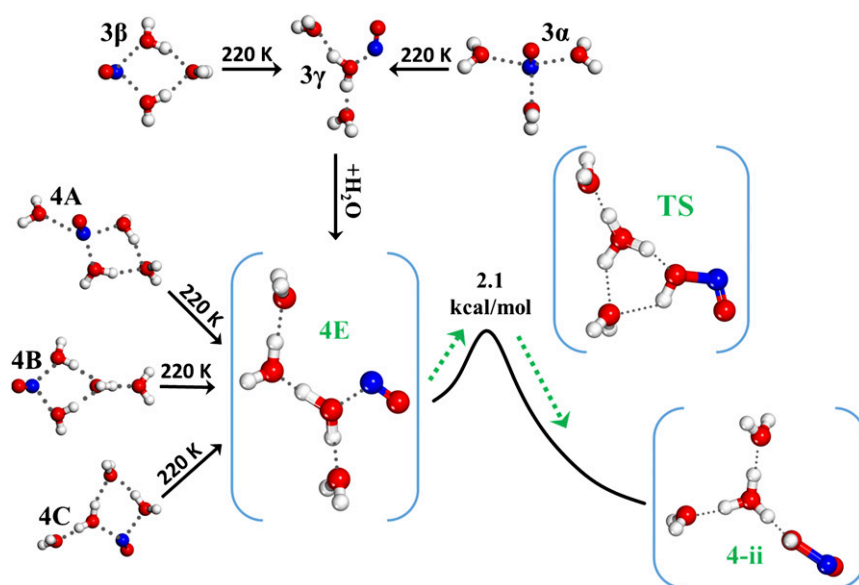


**Fig. 1.** Illustration of the dynamic-driven isomer interconversion observed in AIMD simulations of the trihydrates and tetrahydrates of  $\text{NO}^+$ . The highlighted structures in brackets represent the most likely reaction pathway from the critical (highly populated) isomer 4E to the product isomer 4-ii. White, blue, and red spheres represent hydrogen, nitrogen, and oxygen atoms, respectively.

lowest-lying isomers to the critical chain-like isomers. Furthermore, based on the climbing image nudged-elastic-band method, a more realistic transition state for the formation of hydrated protons and HONO (coexisting in the tetrahydrate) was identified, with the reactant being the critical tetrahydrate  $\text{NO}^+(\text{H}_2\text{O})_4$  isomer. For pentahydrate, two reaction pathways are revealed by the AIMD simulations. Furthermore, the distribution of low-lying isomers at 220 K, including both highly populated critical and less-populated local-minimum isomers, is obtained. In agreement with the results of Relph et al. (16), there is no observed charge transfer between the  $\text{NO}^+$  and the water clusters in the  $n = 1$  or  $n = 2$   $\text{NO}^+(\text{H}_2\text{O})_n$  clusters, indicating that these small clusters are inert. The charge transfer observed for clusters with  $n \geq 3$  suggests the possible formation of HONO from the  $\text{NO}^+(\text{H}_2\text{O})_n$  clusters. However, the population of water clusters decreases rapidly with increasing  $n$  because of the scarcity of the water molecules in the D layer of the ionosphere (17). Therefore, the trihydrate, tetrahydrate, and pentahydrate clusters are most likely the prevailing reactive species for HONO formation in the ionosphere and thus constitute the focus of our AIMD simulations. All the AIMD simulations in this work are performed in the form of the Becke–Lee–Yang–Parr functional (19, 20) with Grimme’s dispersion correction (21) (denoted as BLYP-D method) which can well describe the trend of the charge variation of the  $\text{NO}^+$  hydrates systems (see Fig. S1). Note that our study here is mainly focused on the formation of the HONO species in the hydrates, corresponding to the first step in reaction 1. The detachment of the HONO species from the hydrated proton, which is an endothermic process, is not considered here.

For the trihydrate cluster, the three experimentally detected low-lying isomers (18) are called 3- $\alpha$ , 3- $\beta$ , and 3- $\gamma$  (Fig. 1). Notably, our AIMD simulation shows the isomer interconversion from the two lowest-lying isomers, 3- $\alpha$  and 3- $\beta$ , to 3- $\gamma$  (Fig. S2). In the course of AIMD simulation, the N–O<sub>1</sub> distance decreases from ~2.20 to ~1.90 Å, concurrent with a slight elongation of the O<sub>1</sub>–H<sub>1</sub> and O<sub>1</sub>–H<sub>2</sub> bonds, implying the conversion of isomer 3- $\alpha$  or 3- $\beta$  to the 3- $\gamma$  isomer (Movies S14 and S1B). No isomerization events are observed in the AIMD simulation with the initial 3- $\gamma$  configuration, indicating the high thermal stability of 3- $\gamma$  at 220 K. Hence, the 3- $\gamma$  isomer is expected to exhibit the highest abundance among trihydrate clusters in the D layer of the ionosphere. Moreover, for the

200-ps AIMD simulation of 3- $\gamma$ , no evidence of dissociation of the O–H bonds in water molecules was observed, consistent with the previous experiment-based conclusion (16) that trihydrate clusters do not play a major role in reaction 1.

For the tetrahydrate cluster, the four lowest-lying isomers 4A, 4B, 4C, and 4E (Fig. 1) (18) were selected to investigate their dynamic behaviors at 220 K. As shown in Fig. S3, the O–H bonds of the water molecule directly bound to the  $\text{NO}^+$  are <1.20 Å during the 200-ps AIMD simulations, indicating the absence of HONO-forming reactions in that time period. In contrast, sudden changes in the N–O distance (e.g., at ~26 ps in Fig. S34; the definition of N–O distance is given in the caption of Fig. S3) are observed in all four independent AIMD simulations (black lines in Fig. S3), indicating isomer interconversion. To characterize the degree of isomer interconversion, the bond-orientational order parameter ( $\Psi$ ) given by

$$\Psi = \frac{1}{n} \left| \sum_{j=1}^n e^{in\varphi_{i-j}} \right|$$

is computed, where  $n$  is the total number of atoms  $j$  within a given radius cutoff and  $\varphi_{i-j}$  is the angle between the vector connecting the target atom  $i$  with the neighboring atom  $j$  and the reference vector connecting the target atom  $i$  and the system’s center of mass (marked by the black solid circle in the *Inset* of Fig. 24). Two different target atoms with their corresponding neighboring (source) atom  $j$  were selected to characterize the structural variation: (i) the N atom in the  $\text{NO}^+$  motif with the O atoms in the water molecules as the source of atom  $j$ , and (ii) the O atom (shown by the green sphere in Fig. 24, *Inset*) in the water molecule located at the longer end of the chain structure with the O atoms in the other water molecules that forms a hydrogen bond with the target O atom as the source of atom  $j$ . In chain-like structures, such as isomer 4E, only one O atom exists within 2.80 Å of the N atom, whereas the target O atom only forms one hydrogen bond with the neighboring water molecule. Hence, the logarithms of  $\Psi_{\text{N-O}}$  and  $\Psi_{\text{O-O}}$  take values of zero for isomer 4E. For other isomers, either  $\Psi_{\text{N-O}}$  or  $\Psi_{\text{O-O}}$  is nonzero. Fig. 24 shows the time-dependent order parameters given by the logarithms of  $\Psi_{\text{N-O}}$  (red line) and  $\Psi_{\text{O-O}}$  (black line), with isomer 4A as the initial structure. The disappearance of the red peaks at ~26 ps clearly results from the isomer

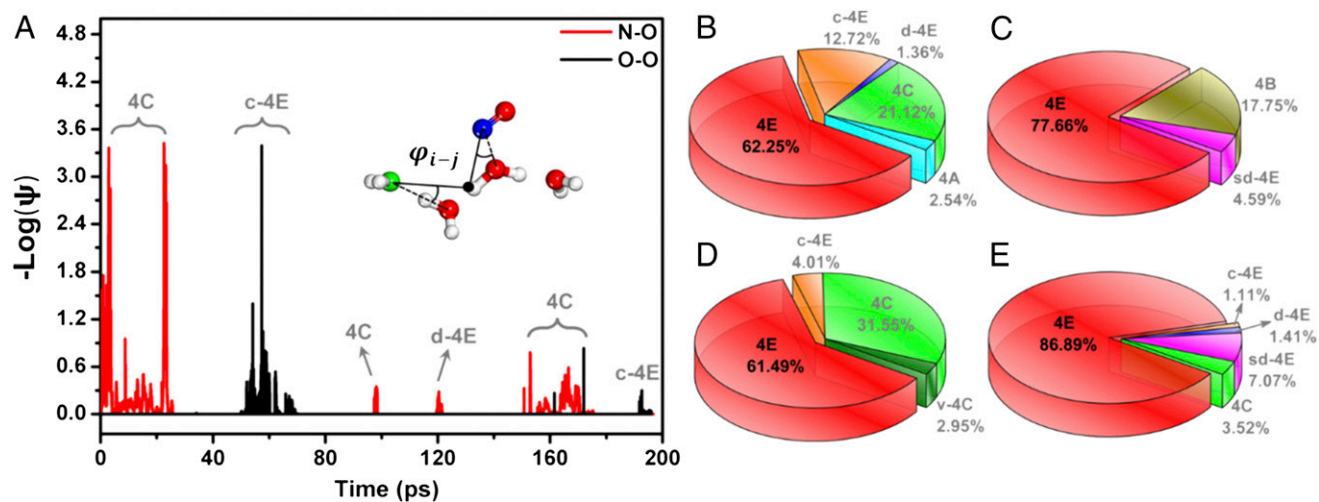


**Fig. 2.** (A) Time evolution of the logarithms of the bond-orientational order parameters  $\Psi_{N-O}$  (red line) and  $\Psi_{O-O}$  (black line). (Inset) Illustration of the angle  $\phi_{i-j}$  used to calculate  $\Psi_{N-O}$  and  $\Psi_{O-O}$ , where white and red spheres represent oxygen and hydrogen atoms, respectively, and blue and green spheres represent the target nitrogen and oxygen atoms, respectively, used to calculate the bond-orientational order parameter. The pie charts in B–E denote the populations of various isomers observed in four independent AIMD simulations with initial structures of 4A, 4B, 4C, and 4E, respectively. The geometric structures of the isomers are given in Fig. S4.

transformation from 4C to 4E (Figs. S34 and S4 and Movie S24). The cyclization of 4E leads to the formation of an additional hydrogen bond with the target O atom, resulting in nonzero values of the logarithm of  $\Psi_{O-O}$  for the ~50–70-ps time period (see c-4E isomer in Fig. S4). The proximity of the N and O atoms of two nearest water molecules (the corresponding isomer is denoted as d-4E in Fig. S4) results in a small red peak at ~120 ps. Similar isomer interconversion is also observed in other AIMD simulations with 4B, 4C, or 4E as the initial structure. The corresponding time-evolution data for  $\Psi_{N-O}$  or  $\Psi_{O-O}$  and associate isomer structures are shown in Figs. S5 and S4, respectively.

The chain-like water structure is the critical structure bridging two different isomers during isomer interconversion. As shown in Fig. 2A and Fig. S5, the zero-value interval between two peaks indicates the appearance of isomer 4E during the isomer conversion. More importantly, the population analysis of each isomer over the entire 200-ps AIMD simulation suggests that the chain-like water structure of 4E is much more abundant than the other isomers (Fig. 2B–E). Specifically, in the four independent AIMD simulations with initial structures of 4A, 4B, 4C, and 4E, the obtained population values are highest for 4E: ~62.25%, 77.66%, 61.49%, and 86.89%, respectively. Note that at 0 K, BLYP-D functional (19, 20; see Supporting Information, Computational Details) predicts that 4E is lower in energy than 4A (i.e., BLYP-D introduces some biases toward 4E over 4A, see Fig. S6 for MP2 results). But, 4E is still about 1 kcal/mol higher in energy than 4B or 4C at the BLYP-D level. At 220 K, 4E becomes the most thermodynamically favorable isomer at the BLYP-D level. Hence, the 4E isomer can be viewed as the critical isomer among the tetrahydrate clusters and plays a critical role in the D layer of the ionosphere.

The HONO-containing tetrahydrate isomer detected experimentally at 5 K (named 4-ii in ref. 16) has nearly the same structure as 4G (Fig. S7). The interconversion between isomer 4-ii and 4G through HONO rotation and flipping of the  $H_3O^+$  groups was frequently observed in the AIMD simulations (Movie S2B). More importantly, no breaking down of the N–O bonds in HONO was observed in the course of the 200-ps AIMD simulation, suggesting that both isomers are highly stable at 220 K. Therefore, the 4-ii isomer can be viewed as the final product of HONO formation, consistent with the experimental detection of 4-ii at 5 K. To confirm this interpretation, we used climbing image nudge-elastic-band calculations (22) to search for the transition state that bridges the

4E and 4-ii isomers. As shown in Fig. 1, the movement of the water molecule at the short end of the chain-like structure toward the long end and the subsequent formation of two H bonds with two neighboring water molecules led to proton transfer between the two neighboring water molecules, giving rise to the transition state (TS in Fig. 1). Upon passing over the TS, the original water molecule near the short end breaks one hydrogen bond while retaining the other hydrogen bond with the protonated species, concurrent with the formation of HONO species. In this cooperative process, the movement of the water molecule at the short end leads to the formation of a cyclic structure, where the two water molecules and the HONO species act as hydrogen-bond acceptors and form a complete solvation shell around the  $H_3O^+$  ion. The formation of such a solvation shell can effectively stabilize the central  $H_3O^+$  ion, a well-established fact in the gas-phase reaction involving ionic clusters (23–26). Due to the stabilization effect, the formation of HONO-containing isomer 4-ii, from the highly populated isomer 4E, entails a low-energy barrier of ~2.1 kcal/mol. Thus, at the ionospheric temperatures (200–220 K), a chemical equilibrium between 4E and the HONO-containing isomers 4-ii is expected to be an important dynamic channel for HONO formation. Note that in our AIMD simulations, the nuclear quantum effect and the hydrogen tunneling effect are not included. In general, the nuclear quantum effect is equivalent to the lowering of density-functional theory (e.g., BLYP-D) temperature of water by certain degrees (27), whereas the hydrogen tunneling would speed up the proton transfer process in our system not included in the AIMD simulations. Nevertheless, the two effects seem to somewhat offset each other and, as a result, may not affect the qualitative reaction mechanism concluded from the AIMD simulations.

Another channel for HONO formation can occur through the pentahydrate  $NO^+(H_2O)_5$ , although the population of pentahydrate clusters is expected to be much lower than that of the tetrahydrate clusters. Here, the lowest-lying four isomers, 5A, 5B, 5D, and 5M (23), are selected as the initial structures in four independent AIMD simulations. In the simulation starting with isomer 5A, no HONO formation or appreciable changes in the N–O and O–H distances were observed within the 200-ps simulation, suggesting that 5A is a highly stable isomer. In contrast, the formation of HONO species is directly observed in the AIMD simulations with initial structures of 5B, 5D, and 5M, indicating that in this case, the HONO-forming reaction has a very low energy barrier. Moreover,



cases (Fig. 3). Again, 5Y changes to 5Γ after a relatively longer period of AIMD run.

In conclusion, we have shown that the tetrahydrate and pentahydrate structures located at the global minima of potential-energy surface cannot be converted directly to HONO species at the 220-K ionospheric temperature. To achieve HONO formation, the lowest-lying isomers of tetrahydrates must first be converted to the highly populated critical isomer 4E in a dynamic fashion at 220 K. Subsequently, the critical isomer 4E can be converted to the HONO-containing product with encountering very low barriers at 220 K, consistent with previous experiment (11, 17). We also confirmed another experimental finding (18) that the 3γ trihydrate cluster is a highly stable nonreactive cluster, even at 220 K (Fig. 1). However, the addition of one water molecule to 3γ can directly lead to the critical 4E isomer. Thus, the chemical equilibrium between 4E and the product 4ii coupled with the thermodynamically favorable conversion process from the three lowest-lying isomers at 0 K—4A, 4B, and 4C—to the 4E isomer at 220 K represents an important dynamic channel for HONO formation in the ionosphere.

Another dynamic channel for HONO formation involves pentahydrate isomers. Upon the addition of one extra water molecule, the formation of HONO can be significantly much faster (11), for example, via a pathway similar to that proposed in the tetrahydrates, namely, via the isomer 5C which contains the motif 4C, followed by the formation of a chain-like water structure akin to 4E and by the bending of the chain to form the product 5Γ. In comparison with the tetrahydrates, the extra water molecule promotes the movement of water molecules, thus leading to the much faster formation of HONO in AIMD simulations. Another possible channel for the formation of HONO could be through the three-armed, star-like precursor isomer 5Y, followed by the combination of a single water molecule with the chain-like water structure to form the product 5Γ. The chemical equilibrium between highly populated 5A or 5Y and 5Γ corresponds to the second dynamic channel for HONO formation in the ionosphere. The discovery of these two dynamic channels brings previously unidentified insights into the HONO formation in the 200–220-K temperature range, a key reaction in the D layer of the ionosphere (17).

1. Lastovicka J, Akmaev RA, Beig G, Bremer J, Emmert JT (2006) Atmosphere. Global change in the upper atmosphere. *Science* 314(5803):1253–1254.
2. Fehsenfeld FC, Ferguson EE (1969) Origin of water cluster ions in the D region. *J Geophys Res* 74:2217–2222.
3. Fehsenfeld FC, Mosesman M, Ferguson EE (1971) Ion-molecule reactions in  $\text{NO}^+ \cdot \text{H}_2\text{O}$  system. *J Chem Phys* 55(5):2120–2125.
4. Lineberger WC, Puckett LJ (1969) Hydrated positive ions in nitric-oxide-water afterglows. *Phys Rev* 187:286–291.
5. Mollner AK, et al. (2010) Rate of gas phase association of hydroxyl radical and nitrogen dioxide. *Science* 330(6004):646–649.
6. Su H, et al. (2011) Soil nitrite as a source of atmospheric HONO and OH radicals. *Science* 333(6049):1616–1618.
7. Li X, et al. (2014) Missing gas-phase source of HONO inferred from Zeppelin measurements in the troposphere. *Science* 344(6181):292–296.
8. Vöhringer-Martinez E, et al. (2007) Water catalysis of a radical-molecule gas-phase reaction. *Science* 315(5811):497–501.
9. Gerber RB, et al. (2015) Computational studies of atmospherically-relevant chemical reactions in water clusters and on liquid water and ice surfaces. *Acc Chem Res* 48(2):399–406.
10. Beyer M, Williams ER, Bondybey VE (1999) Unimolecular reactions of dihydrated alkaline earth metal dications  $\text{M}_2+(\text{H}_2\text{O})_2$ ,  $\text{M} = \text{Be}, \text{Mg}, \text{Ca}, \text{Sr}$ , and  $\text{Ba}$ : Salt-bridge mechanism in the proton-transfer reaction  $\text{M}_2+(\text{H}_2\text{O})_2 \rightarrow \text{MOH}^+ + \text{H}_3\text{O}^+$ . *J Am Chem Soc* 121(7):1565–1573.
11. Eyet N, et al. (2011) The importance of  $\text{NO}^+(\text{H}_2\text{O})_4$  in the conversion of  $\text{NO}^+(\text{H}_2\text{O})_n$  to  $\text{H}_3\text{O}^+(\text{H}_2\text{O})_n$ : I. Kinetics measurements and statistical rate modeling. *J Phys Chem A* 115(26):7582–7590.
12. Hammam E, Lee EPF, Dyke JM (2001) Ab initio molecular orbital calculations on  $\text{NO}^+(\text{H}_2\text{O})_n$  cluster ions. 2. Thermodynamic values for stepwise hydration and nitrous acid formation. *J Phys Chem A* 105(23):5528–5534.
13. Le HM, Raff LM (2008) Cis- $\rightarrow$ trans, trans- $\rightarrow$ cis isomerizations and N-O bond dissociation of nitrous acid (HONO) on an ab initio potential surface obtained by novelty sampling and feed-forward neural network fitting. *J Chem Phys* 128(19):194310.
14. Yeh LI, Okumura M, Myers JD, Price JM, Lee YT (1989) Vibrational spectroscopy of the hydrated hydronium cluster ions  $\text{H}_3\text{O}^+(\text{H}_2\text{O})_N$  ( $N = 1, 2, 3$ ). *J Chem Phys* 91(12):7319–7330.
15. Ye L, Cheng H-P (1998) A quantum molecular dynamics study of the properties of  $\text{NO}^+(\text{H}_2\text{O})_n$  clusters. *J Chem Phys* 108(5):2015–2023.
16. Relph RA, et al. (2010) How the shape of an H-bonded network controls proton-coupled water activation in HONO formation. *Science* 327(5963):308–312.
17. Siefermann KR, Abel B (2010) Chemistry. Ion chemistry mediated by water networks. *Science* 327(5963):280–281.
18. Asada T, Nagaoka M, Koseki S (2011) Ab initio electron correlated studies on the intracuster reaction of  $\text{NO}^+(\text{H}_2\text{O})_n \rightarrow \text{H}_3\text{O}^+(\text{H}_2\text{O})_{(n-2)}(\text{HONO})$  ( $n = 4$  and  $5$ ). *Phys Chem Chem Phys* 13(4):1590–1596.
19. Becke AD (1998) Density-functional exchange-energy approximation with correct asymptotic behavior. *Phys Rev A* 38(6):3098–3100.
20. Lee C, Yang W, Parr RG (1988) Development of the Colle-Salvetti correlation-energy formula into a functional of the electron density. *Phys Rev B Condens Matter* 37(2):785–789.
21. Grimme S, Antony J, Ehrlich S, Krieg H (2010) A consistent and accurate ab initio parametrization of density functional dispersion correction (DFT-D) for the 94 elements H-Pu. *J Chem Phys* 132(15):154104.
22. Henkelman G, Uberuaga BP, Jonsson H (2000) A climbing image nudged elastic band method for finding saddle points and minimum energy paths. *J Chem Phys* 113(22):9901–9904.
23. Botti A, Bruni F, Imberti S, Ricci MA, Soper AK (2005) Solvation shell of  $\text{H}^+$  ions in water. *J Mol Liq* 117(1–3):77–79.
24. Miller DJ, Lisy JM (2006) Mimicking solvent shells in the gas phase. II. Solvation of  $\text{K}^+$ . *J Chem Phys* 124(2):024319.
25. Raugai S, Klein ML (2001) Dynamics of water molecules in the  $\text{Br}^-$  solvation shell: An ab initio molecular dynamics study. *J Am Chem Soc* 123(38):9484–9485.
26. Stace AJ (2002) Metal ion solvation in the gas phase: The quest for higher oxidation states. *J Phys Chem A* 106(35):7993–8005.
27. Morrone JA, Car R (2008) Nuclear quantum effects in water. *Phys Rev Lett* 101(1):017801.
28. VandeVondele J, et al. (2005) QUICKSTEP: Fast and accurate density functional calculations using a mixed Gaussian and plane waves approach. *Comput Phys Commun* 167(2):103–128.
29. VandeVondele J, Hutter J (2007) Gaussian basis sets for accurate calculations on molecular systems in gas and condensed phases. *J Chem Phys* 127(11):114105.
30. Hartwigsen C, Goedecker S, Hutter J (1998) Relativistic separable dual-space Gaussian pseudopotentials from H to Rn. *Phys Rev B* 58(7):3641–3662.
31. Goedecker S, Teter M, Hutter J (1996) Separable dual-space Gaussian pseudopotentials. *Phys Rev B Condens Matter* 54(3):1703–1710.
32. Boese AD, Doltsinis NL, Handy NC, Sprik M (2000) New generalized gradient approximation functionals. *J Chem Phys* 112(4):1670–1678.
33. Yoo S, Xantheas SS (2011) Communication: The effect of dispersion corrections on the melting temperature of liquid water. *J Chem Phys* 134(12):121105.
34. Nose S (1984) A unified formulation of the constant temperature molecular-dynamics methods. *J Chem Phys* 81(1):511–519.
35. Hoover WG (1985) Canonical dynamics: Equilibrium phase-space distributions. *Phys Rev A* 31(3):1695–1697.
36. Mills G, Jonsson H, Schenter GK (1995) Reversible work transition-state theory - Application to dissociative adsorption of hydrogen. *Surf Sci* 324(2–3):305–337.

# Supporting Information

He et al. 10.1073/pnas.1601651113

## Computational Details

The Born–Oppenheimer AIMD simulations are performed by using the Gaussian and plane-wave method as implemented in the CP2K Quickstep package (28). The valence electrons are treated with the wave functions expanded in a double- $\zeta$  Gaussian basis set combined with an auxiliary basis set (29), whereas the core electrons are treated with the Goedecker–Teter–Hutter norm-conserved pseudopotentials (30, 31). The plane-wave cutoff is set as 300 Rydberg. The electron exchange and correlation interactions are described with the Becke–Lee–Yang–Parr (BLYP) functional (19, 20) and the London dispersion interaction is considered via the employment of Grimme’s dispersion correction method (21). The BLYP-D functional has been widely used in water-based systems owing to its reasonably accurate description of the structural and dynamic properties of the systems (32, 33). Also, it can well describe the trend of the charge variation of the  $\text{NO}^+$  hydrate systems (Fig. S1). The electrostatic energy is computed via the Ewald summation with the inclusion of the neutralizing background charge for compensating the charge of the hydrate

system. A large supercell ( $30 \times 30 \times 30 \text{ \AA}^3$ ) is selected so that the interaction between two neighboring water clusters is negligible.

For all AIMD simulations, the constant-volume and constant-temperature ensemble is adopted with a time step of 1.0 fs. The simulation temperature is controlled at  $\sim 220 \text{ K}$  (the upper limit of temperature at the ionosphere D layer) through the Nosé–Hoover chain method (34, 35). The length and number of multiple time steps of the Nose–Hoover chain are set to the default values (3, 2), and the time constant and order of the Yoshida integrator used for the thermostat are 300 fs and 3, respectively. These parameters are reasonable for the present AIMD simulations. All of the snapshot structures and movies from AIMD simulations are generated by using Visual Molecular Dynamics (VMD) code (Version 1.9.2). The transition state is determined by using the climbing image nudged-elastic-band (CI-NEB) method (22, 36). Nine replicas are applied for each CI-NEB computation with the spring force being less than  $0.02 \text{ eV/\AA}$ . The vibrational frequencies are calculated to confirm only one imaginary frequency exists for the transition state.

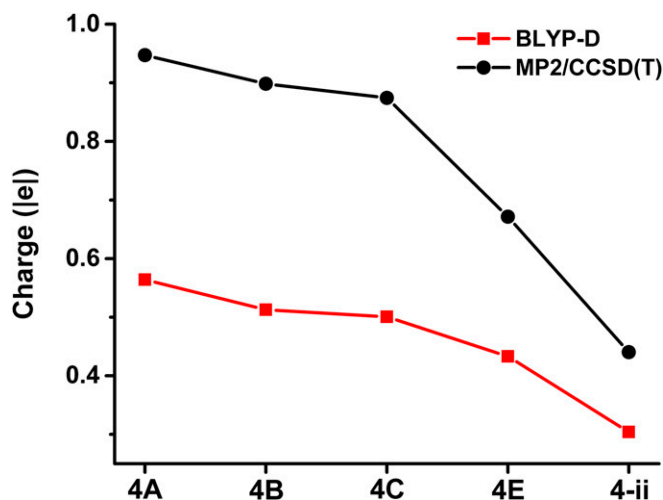


Fig. S1. Charge on the NO varies with the isomers for tetrahydrates on the basis of the Mullikan charge analysis at the BLYP-D and the CCSD(T)/aug-cc-pVTZ//MP2/aug-cc-pVTZ levels of theory [here, CCSD(T) and MP2 refer to the coupled-cluster method with singlet, doublet, and triplet excitations and the second-order Møller–Plesset perturbation theory, respectively]. The CCSD(T)//MP2 denotes that the structure is optimized at the MP2/aug-cc-pVTZ level, whereas the charge analysis is performed at the CCSD(T)/aug-cc-pVTZ level.



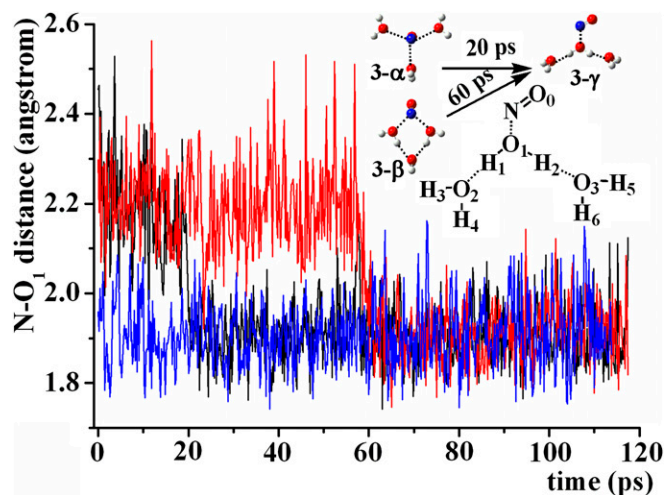


Fig. S2. N-O<sub>1</sub> distance change with time for isomers 3- $\alpha$  (black), 3- $\beta$  (red), and 3- $\gamma$  (blue). Time required for the structural transformation from 3- $\alpha$  and 3- $\beta$  to 3- $\gamma$ . The atomic label is given. Note that both H<sub>1</sub> and H<sub>2</sub> bind with two different water molecules via H-bond arrangement, which is the so-called "symmetrical H bond."

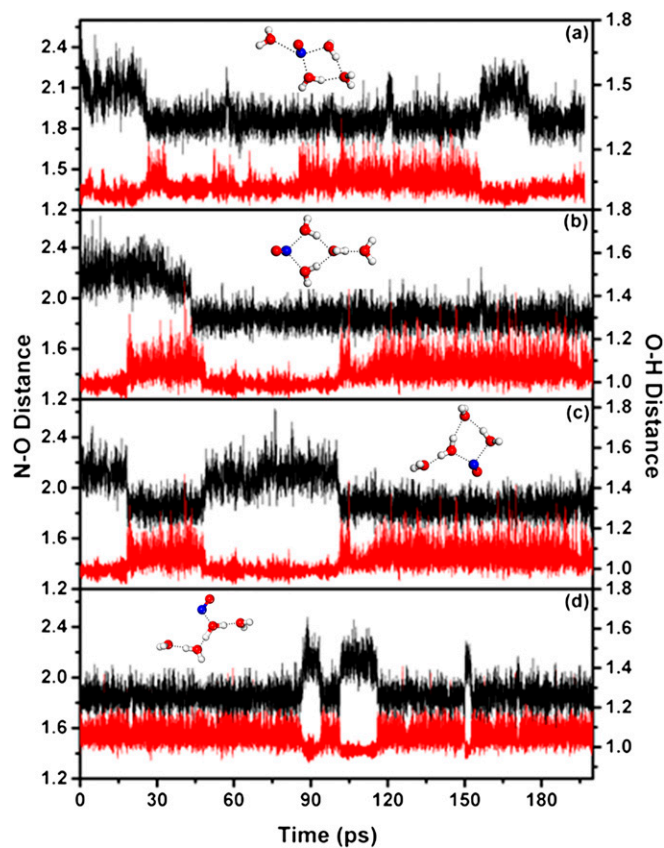
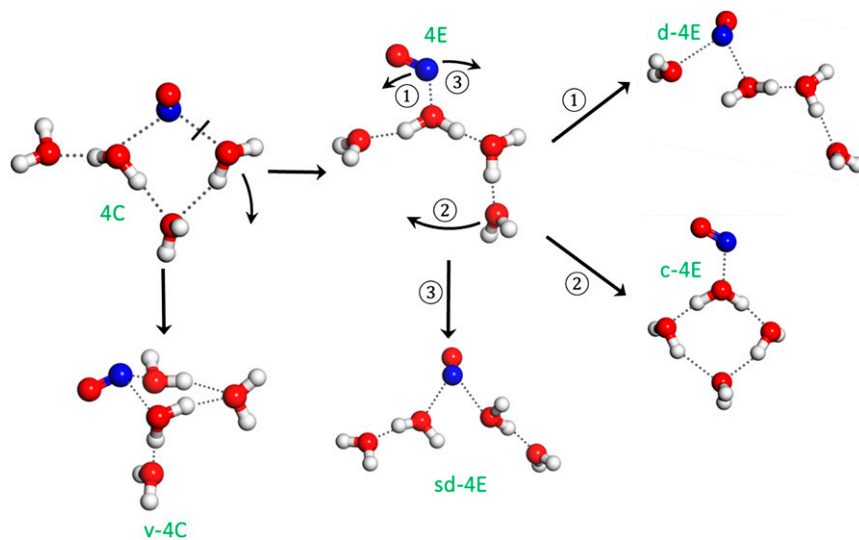
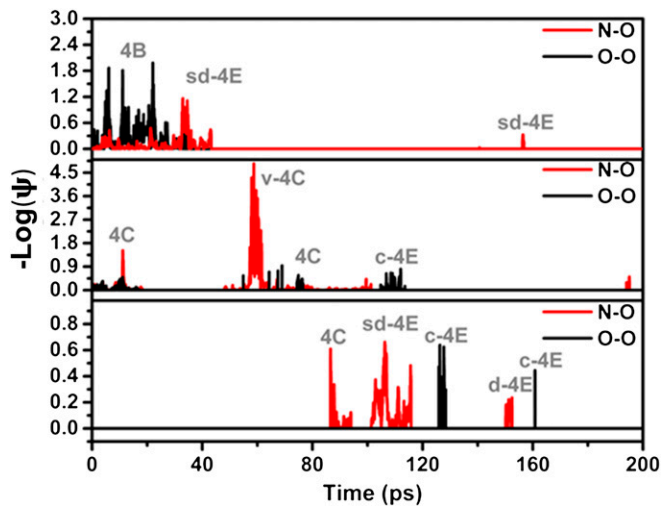


Fig. S3. Time evolution of the N-O (black line) (where O is the O atom of the nearest H<sub>2</sub>O molecule next to the N atom of the NO<sup>+</sup> ion) and the O-H (red line) (where O-H refers to the averaged O-H bond length for the water molecule nearest to the NO<sup>+</sup> ion) distances for the AIMD simulations of NO<sup>+</sup>(H<sub>2</sub>O)<sub>4</sub> clusters with different initial isomer: (A) isomer 4A, (B) isomer 4B, (C) isomer 4C, and (D) isomer 4E. (Inset) Images represent the initial structures used in each AIMD simulation.

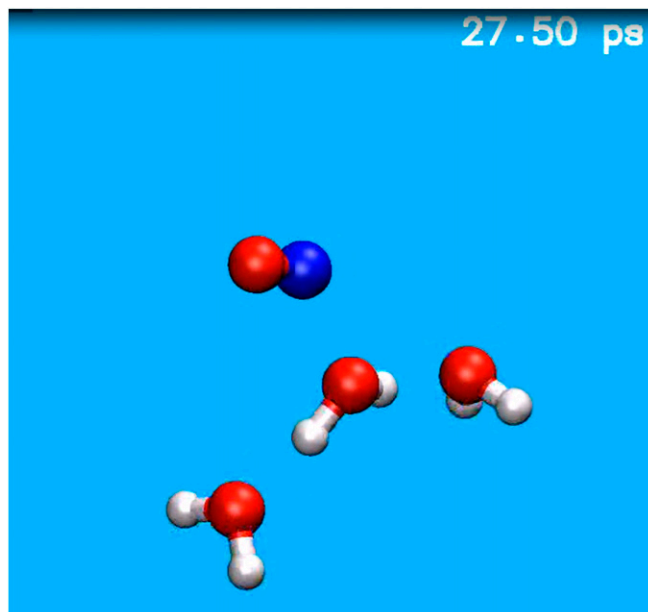


**Fig. S4.** Geometrical structures of the observed isomers in the AIMD simulation with isomer 4A as the initial structure. The white, blue, and red spheres represent the hydrogen, nitrogen, and oxygen atoms. The arrows and three pairs of circled numbers indicate several possible shifting directions of molecules and corresponding interconversion of isomers.



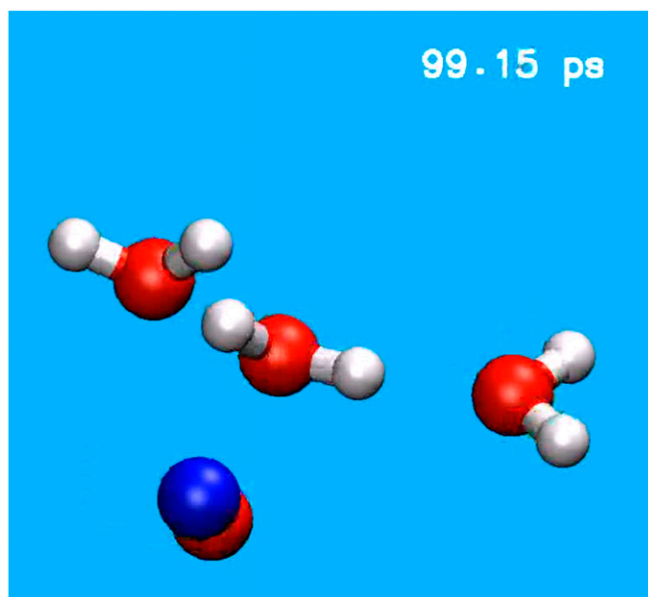
**Fig. S5.** Time evolution of the logarithm of the bond-orientational order parameter  $\Psi_{N-O}$  (red lines) and  $\Psi_{O-O}$  (black lines) for the AIMD simulations starting from isomer 4B (Top), 4C (Middle), and 4E (Bottom), respectively.





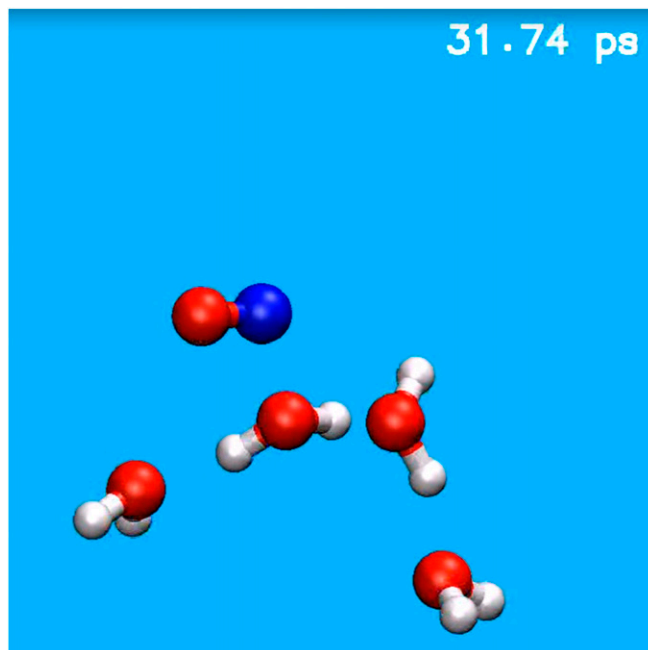
Movie S1A. Conversion of isomer 3 $\alpha$  to 3 $\gamma$ .

[Movie S1A](#)



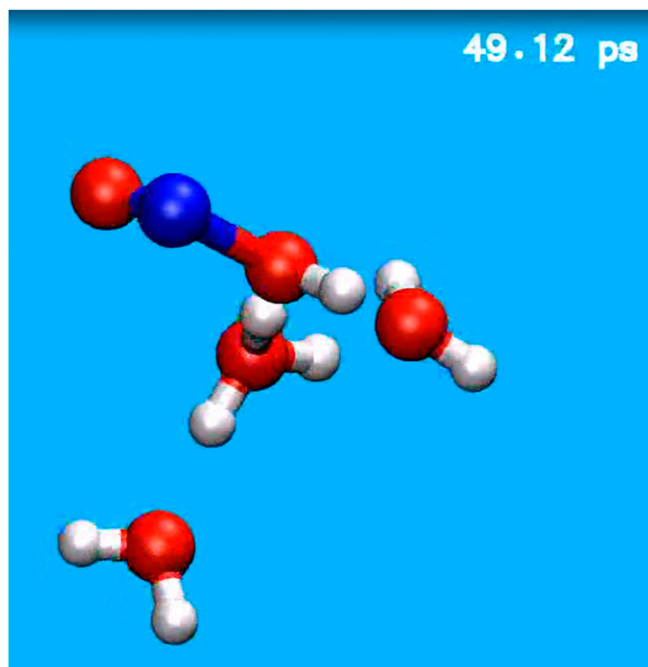
Movie S1B. Conversion of isomer 3 $\beta$  to 3 $\gamma$ .

[Movie S1B](#)



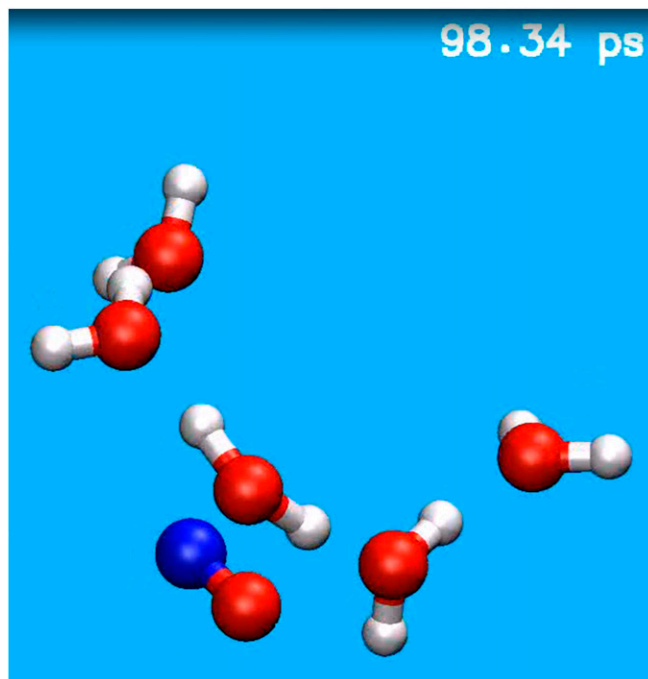
Movie S2A. Conversion of isomer 4C to 4E.

[Movie S2A](#)



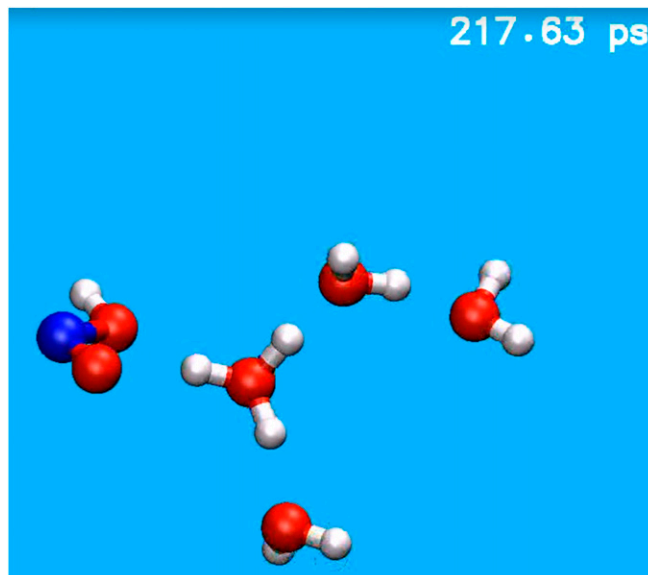
Movie S2B. Isomer interconversion among the HONO-containing isomer 4-ii and 4G.

[Movie S2B](#)



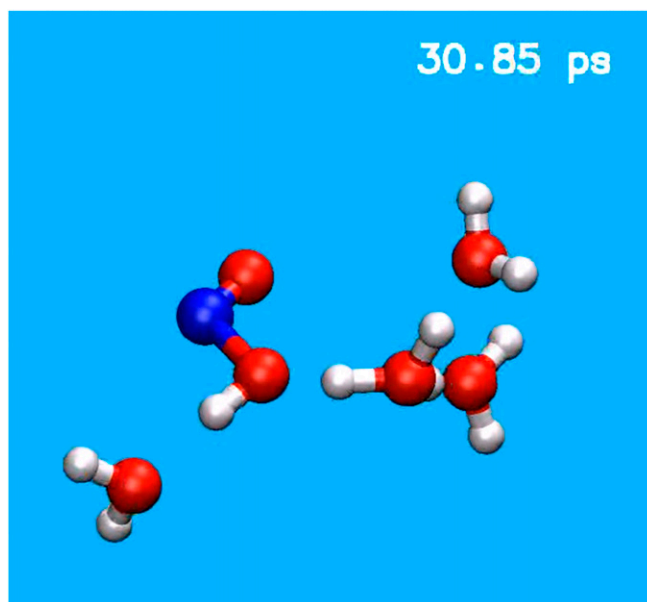
**Movie S3A.** Conversion from the water-loop-containing isomer  $5\sigma$  to the highly populated isomer  $5\lambda$  in the AIMD simulation starting at isomer  $5B$ .

[Movie S3A](#)



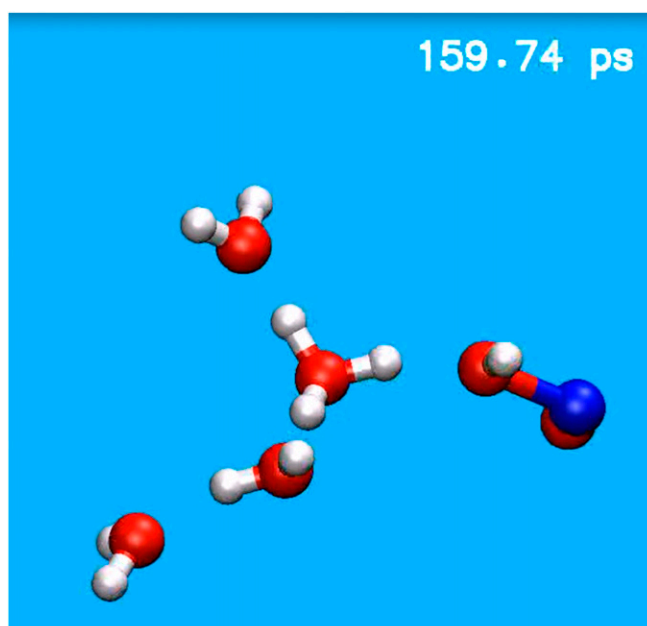
**Movie S3B.** Formation of the product isomer  $5\Gamma$  from the highly populated isomer  $5\lambda$  in the AIMD simulation starting at isomer  $5B$ .

[Movie S3B](#)



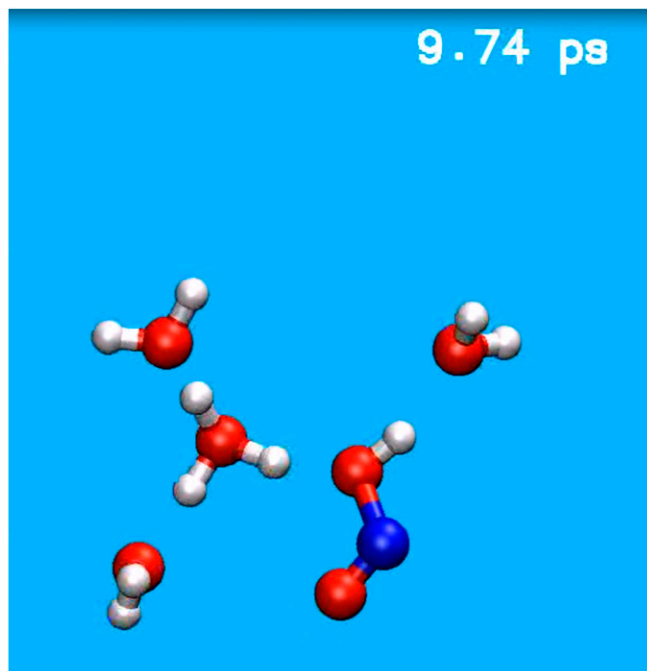
**Movie S3C.** Conversion from the water-loop-containing isomer  $5\sigma$  to the highly populated isomer  $5Y$  in the AIMD simulation starting from isomer  $5D$ .

[Movie S3C](#)



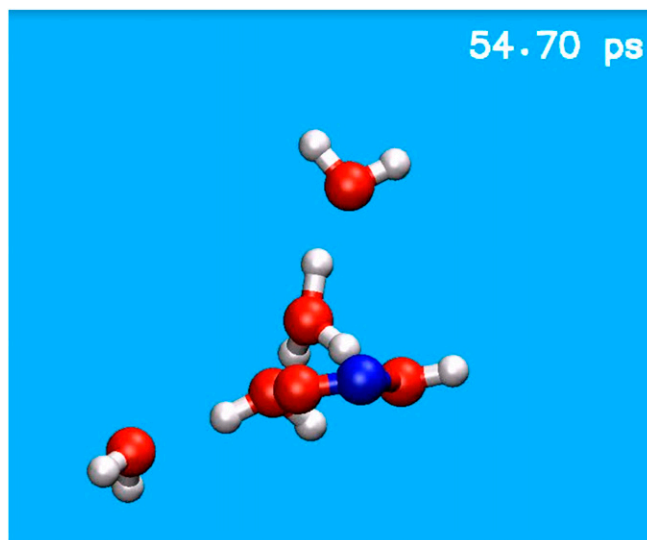
**Movie S3D.** Formation of the product isomer  $5\Gamma$  from the highly populated isomer  $5Y$  in the AIMD simulation starting from isomer  $5D$ .

[Movie S3D](#)



**Movie S3E.** Conversion from the water-loop-containing isomer 5M to the highly populated isomer 5Y in the AIMD simulation starting from isomer 5M.

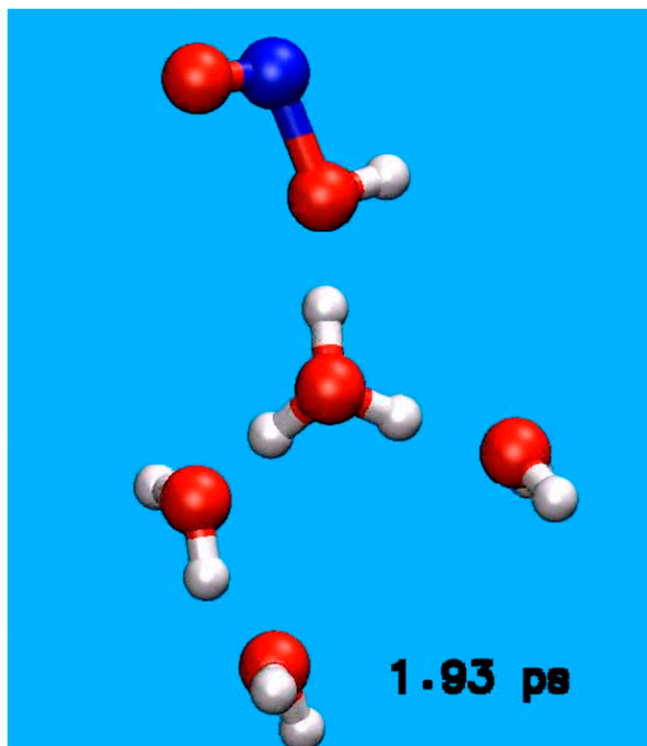
[Movie S3E](#)



**Movie S3F.** Formation of the product isomer 5Γ from the highly populated isomer 5Y in the AIMD simulation starting from isomer 5M.

[Movie S3F](#)





Movie S3G. AIMD simulation of isomer 5M with the time step set as 0.1 fs.

[Movie S3G](#)